NJC

ROYAL SOCIETY OF CHEMISTRY

PAPER

View Article Online
View Journal | View Issue

Cite this: *New J. Chem.*, 2021, 45, 13869

Bright photo- and triboluminescence of centrosymmetric Eu(III) and Tb(III) complexes with phosphine oxides containing azaheterocycles†

Yuliya A. Bryleva, * Alexander V. Artem'ev, Ludmila A. Glinskaya, Mariana I. Rakhmanova, Denis G. Samsonenko, Vladislav Yu. Komarov, Maxim I. Rogovoy and Maria P. Davydova

Received 18th May 2021,
Accepted 25th June 2021

DOI: 10.1039/d1nj02441h

rsc.li/njc

Six centrosymmetric mononuclear Eu^{3+} and Tb^{3+} complexes of the type $[LnL_2(hfac)_3]$ have been synthesized employing diphenyl(pyridin-2-yl)phosphine oxide ($Ph_2P(O)Py$), diphenyl(pyridimin-2-yl)phosphine oxide ($Ph_2P(O)Pym$), and diphenyl(pyrazin-2-yl)phosphine oxide ($Ph_2P(O)Pyr$) as supporting ligands (L). The complexes $[LnL_2(hfac)_3]$ (L = $Ph_2P(O)Py$ and $Ph_2P(O)Pyr$) comprise an eight-coordinate Ln^{3+} ion with two monodentate O-donor phosphine oxides and three bidentate $hfac^-$ anions. In the $[Ln\{Ph_2P(O)Pym\}_2(hfac)_3]$ complexes, the Ln^{3+} ion is nine-coordinated by three bidentate $hfac^-$ anions and two $Ph_2P(O)Pym$ ligands, one of which is bound to Ln in a N,O-bidentate chelating mode, and the other acts as a monodentate O-donor ligand. The complexes display bright solid-state photoluminescence with emission quantum yields up to 56%. The integral intensity of $^5D_0 \rightarrow {}^7F_2$ transition in the emission spectra of the Eu(III) complexes strongly depends on the coordination environment of the Eu^{3+} ion. The asymmetric coordination geometry around Eu^{3+} results in the large radiative rate constants. The crystals of the Eu(III) and Tb(III) complexes exhibit triboluminescence upon breaking under ambient conditions. The relationship between the triboluminescent properties and crystal structures of the complexes is discussed.

1. Introduction

Phosphine oxides are widely used for the design and synthesis of luminescent lanthanide (Ln) coordination compounds due to their strong coordination ability to Ln^{3+} ions, and the attractive photophysical properties of complexes based on these ligands.[1–4] The phosphine oxides bearing fluorophore moieties have proven to be efficient sensitizers of the Ln(III) luminescence with high quantum yields and long luminescence lifetimes.[5–15] Moreover, some Ln complexes based on phosphine oxides exhibit remarkable photophysical properties such as triboluminescence,[16–23] and luminescence depending on temperature,[24–28] solvent,[29,30] or counterion.[31]

Importantly, the ability to incorporate a wide variety of groups into the structures of phosphine oxides gives enormous scope to the tuning of the properties of the resulting complexes. In particular, the introduction of azaheterocyclic moieties into the phosphine oxides is one of the promising approaches for the preparation of potentially polydentate N,O-donor ligands. Phosphine oxides bearing N-heterocyclic rings attract attention as ligands for Ln(III) complexes due to their distinguished photophysical properties,[32,33] and also due to their ability to discriminate ions of f-elements by their size.[1] Some Ln(III) complexes with these "hard-and-soft" ligands show intense solvent and counter-ion dependent luminescence.[34–37] However, in most of these complexes the nitrogen atoms of N-heterocycle-based phosphine oxides are not involved in coordination with the Ln^{3+} ions and bind to the metal centers only *via* the P=O groups.[33,38,39]

It should be noted that most phosphine oxide-based complexes endowed with outstanding luminescence properties contain fluorinated β-diketonate anions, which are known as efficient photosensitizers of Ln^{3+} ions, especially Eu^{3+} ones.[1] The presence of fluorine atoms in these ligands significantly suppresses vibrational relaxation, thereby strongly enhancing the quantum performance of the Ln(III) luminescence. The polyfluorinated moieties are also responsible for enhanced volatility, lipophilicity and solubility of the complexes, and may play a role in the manifestation of triboluminescence.[18,19] The use of fluorinated β-diketonate anions in combination with phosphine oxide ligands in the Ln(III) coordination sphere is a promising approach for the design of efficient emitters. Through this design strategy, a

Nikolaev Institute of Inorganic Chemistry, Siberian Branch of the Russian Academy of Sciences, 3, Academician Lavrentiev Avenue, Novosibirsk 630090, Russian Federation. E-mail: bryleva@niic.nsc.ru

† Electronic supplementary information (ESI) available. CCDC 2078495–2078497. For ESI and crystallographic data in CIF or other electronic format see DOI: 10.1039/d1nj02441h

number of Ln(III) β-diketonate complexes containing mono- or diphosphine dioxides showing photo- and triboluminescence have been reported.[16,18,19,22,33] Triboluminescent activity makes such complexes very attractive for applications as damage and pressure sensors.[40] The study of triboluminescent complexes is also important from a fundamental viewpoint, because the exact reasons for the origin of triboluminescence are not yet fully understood. The ability of the Ln^{3+} complexes to generate triboluminescence is often associated with a contribution from the piezoelectric effect upon breaking non-centrosymmetric bulk crystals.[41–44] Meanwhile, efficient centrosymmetric triboluminescent Ln(III) complexes were also reported.[20,21] It has also been suggested that the disorder of ligands may be responsible for the triboluminescent activity of lanthanide complexes.[45] Therefore, since there is not currently an unambiguous interpretation of the Ln(III) excitation mechanism, studies of the relationships between the structure and triboluminescence properties of lanthanide coordination compounds are of great interest.

Here, we have designed and synthesized a series of bright photo- and triboluminescent $[LnL_2(hfac)_3]$ complexes (Ln = Eu, Tb) supported by tertiary phosphine oxides (L) bearing pyridine, pyrimidine, or pyrazine moieties. The effect of the nature of the N-heterocycle incorporated in phosphine oxide on the structure and photoluminescence properties of the complexes has been investigated. Moreover, the relationship between triboluminescence properties and crystal structures of the complexes is discussed, which will contribute to the understanding of this type of luminescence.

2. Experimental part

2.1. Reagents

All reagents and solvents were commercially available and were used without additional purification. The compounds were synthesized using $Tb(NO_3)_3{\cdot}6H_2O$, acetone, CH_2Cl_2 and MeOH (chemically pure), $Eu(NO_3)_3{\cdot}6H_2O$ (pure), Et_2O (pure for analysis), EtOH (rectified), and 30% aqueous H_2O_2. $[Ln(hfac)_3(H_2O)_2]$ (Ln = Eu, Tb) were prepared according to ref. 46. The complexes $[Ln(Ph_3PO)_2(hfac)_3]$ (Ln = Eu, Tb) were prepared following a known procedure.[47] 2-(Diphenylphosphino)pyridine was used as purchased (97%, Sigma-Aldrich), and 2-(diphenylphosphino)-pyrazine was prepared according to the reported technique.[48] Diphenyl(pyridimin-2-yl)phosphine oxide ($Ph_2P(O)Pym$) was prepared by a procedure reported in ref. 49.

2.2. Synthesis

Synthesis of diphenyl(pyridin-2-yl)phosphine oxide ($Ph_2P(O)Py$). 30% aqueous H_2O_2 (0.2 mL) was added to a solution of 2-(diphenylphosphino)pyridine (0.527 g, 2 mmol) in acetone (30 mL) at room temperature. After stirring for 20 min the mixture was diluted with distilled H_2O (20 mL) and extracted with CH_2Cl_2 (3 × 30 mL), then the organic layer was washed with distilled H_2O (20 mL), dried over Na_2SO_4 and evaporated *in vacuo* to give a white powder of $Ph_2P(O)Py$. Yield: 0.450 g (80%). The ^1H and ^{31}P NMR spectra correspond to the literature data.[50] Found: C, 73.3; H, 5.0. Calcd for $C_{17}H_{14}NOP$ (279.27): C, 73.1; H, 5.1. IR (KBr pellets, ν/cm^{-1}): 3521w, 3449w, 3228m, 3060w, 2822w, 1635w, 1591w, 1573m, 1482w, 1437s, 1374w, 1309w, 1276w, 1192s, 1141m, 1122s, 1099m, 1085w, 1070w, 1044w, 1027w, 989w, 869w, 845w, 773w, 745s, 745s, 724s, 692s, 620w, 542s, 501w, 455w, 443w (Fig. S1, ESI†).

Synthesis of diphenyl(pyrazin-2-yl)phosphine oxide ($Ph_2P(O)Pyr$). 30% aqueous H_2O_2 (0.3 mL) was added to a solution of 2-(diphenylphosphino)pyrazine (793 mg, 3 mmol) in acetone (30 mL) at room temperature. After stirring for 30 min, the mixture was diluted with distilled H_2O (20 mL) and extracted with CH_2Cl_2 (3 × 30 mL). The combined extract was washed with distilled H_2O (20 mL), dried over Na_2SO_4 and evaporated *in vacuo* to give an off-white powder of $Ph_2P(O)Pyr$. Yield: 0.650 g (77%). ^1H NMR (500.13 MHz, $CDCl_3$, 23 °C) δ 9.41 (t, J = 1.5 Hz, 1H, C_3H in Pyr), 8.76–8.66 (m, 2H, $C_{4,5}H$ in Pyr), 7.93–7.80 (m, 4H, Ph), 7.59–7.52 (m, 2H, Ph), 7.47 (tdd, J = 8.2, 3.0, 1.3 Hz, 4H, Ph). Found: C, 68.5; H, 4.9. Calcd for $C_{16}H_{13}N_2OP$ (280.26): C, 68.6; H, 4.7. IR (KBr pellets, ν/cm^{-1}): 3525w, 3459w, 3258w, 3060w, 1642w, 1589w, 1573w, 1563w, 1482w, 1455w, 1438m, 1424w, 1313w, 1277w, 1201m, 1143w, 1118m, 1099w, 1081w, 1069w, 1044w, 1027w, 990w, 925w, 903w, 862w, 845w, 771w, 757w, 744m, 735s, 722s, 619w, 540s, 497m, 447w (Fig. S1, ESI†).

General synthetic procedure for the preparation of complexes 1–6. A solution of $Ph_2P(O)Py$, $Ph_2P(O)Pym$ or $Ph_2P(O)Pyr$ (0.1 mmol, 0.028 g) in EtOH–Et_2O (2 : 1, 5 mL) for **1** and **2** and in MeOH (3 mL) for **3–6** was added to a solution of $[Ln(hfac)_3(H_2O)_2]$ (0.05 mmol, 0.040 g) in EtOH–Et_2O (2 : 1, 2 mL) for **1** and **2** and in MeOH (2 mL) for **3–6** upon stirring. Slow evaporation of the resulting solution at room temperature afforded colorless crystals suitable for single crystal X-ray analysis after 2–3 days. The crystals were filtered off, washed with EtOH for **1** and **2** and with MeOH for **3–6**, and were dried *in vacuo* at room temperature.

*$[Eu\{Ph_2P(O)Py\}_2(hfac)_3]$ (**1**).* Yield: 0.045 g (67%). Found: C, 43.6; H, 2.4; N, 2.0%; F, 25.0%. Calcd for $C_{49}H_{31}N_2F_{18}O_8P_2Eu$ (1331.7): C, 44.2; H, 2.3; N, 2.1%; F, 25.7%. FT-IR (KBr pellets, ν/cm^{-1}): 3420w, 3065w, 1653s, 1593w, 1576w, 1556m, 1528m, 1496s, 1439m, 1427w, 1344w, 1320w, 1255s, 1199s, 1171s, 1146s, 1098s, 1046w, 1029w, 998w, 991w, 950w, 848w, 797m, 773w, 740m, 726m, 693m, 660m, 618w, 583m, 543s, 460w, 448w, 421w (Fig. S1, ESI†).

*$[Tb\{Ph_2P(O)Py\}_2(hfac)_3]$ (**2**).* Yield: 0.055 g (83%). Calcd for $C_{49}H_{31}N_2F_{18}O_8P_2Tb$ (1338.6): C, 44.0; H, 2.3; N, 2.1%; F, 25.5%. Found: C, 43.4; H, 2.3; N, 2.0%; F, 25.1%. FT-IR (KBr pellets, ν/cm^{-1}): 3420w, 3065w, 1650s, 1592w, 1575w, 1555m, 1516s, 1481s, 1472s, 1439s, 1427w, 1345w, 1320w, 1256s, 1125s, 1198s, 1171s, 1146s, 1095s, 1045w, 1029w, 998w, 991w, 951w, 930w, 894w, 853w, 791m, 772w, 740s, 727s, 692m, 669s, 617w, 580m, 542s, 458w, 448w, 423w (Fig. S1, ESI†).

*$[Eu\{Ph_2P(O)Pym\}_2(hfac)_3]$ (**3**).* Yield: 0.039 g (54%). Found: C, 41.9; H, 2.9; N, 4.2%; F, 25.2%. Calcd for $C_{47}H_{29}N_4F_{18}O_8P_2Eu$ (1333.6): C, 42.3; H, 2.2; N, 4.2%; F, 25.6%. FT-IR (KBr pellets, ν/cm^{-1}): 3432w, 3065w, 1656m, 1614w, 1592w, 1556m, 1527m,

1506m, 1489w, 1440w, 1392w, 1345w, 1321w, 1256s, 1200s, 1180m, 1165s, 1148s, 1123m, 1099w, 1073w, 1029w, 998w, 990w, 950w, 806w, 794w, 765w, 746w, 727w, 692w, 661m, 635w, 615w, 585w, 560m, 554m, 539m, 460w, 447w, 410w (Fig. S1, ESI†).

*[Tb{Ph$_2$P(O)Pym}$_2$(hfac)$_3$] (**4**).* Yield: 0.038 g (57%). Found: C, 41.5; H, 2.0; N, 4.0%; F, 24.9%. Calcd for $C_{47}H_{29}N_4F_{18}O_8P_2Tb$ (1340.6): C, 42.1; H, 2.2; N, 4.2%; F, 25.5%. FT-IR (KBr pellets, ν/cm^{-1}): 3430w, 3065w, 1660s, 1613w, 1592w, 1556s, 1528s, 1506s, 1487m, 1440m, 1393m, 1345w, 1321w, 1257s, 1215s, 1198s, 1165s, 1145s, 1121s, 1098m, 1071w, 1031w, 998w, 989w, 950w, 806w, 794m, 764w, 746m, 727m, 693m, 661s, 634w, 618w, 585m, 561m, 551m, 537s, 460w, 441w, 410w (Fig. S1, ESI†).

*[Eu{Ph$_2$P(O)Pyr}$_2$(hfac)$_3$] (**5**).* Yield: 0.047 g (70%). Found: C, 42.0; H, 2.1; N, 4.0%; F, 25.1%. Calcd for $C_{47}H_{29}N_4F_{18}O_8P_2Eu$ (1333.6): C, 42.3; H, 2.2; N, 4.2%; F, 25.6%. FT-IR (KBr pellets, cm^{-1}): 3440w, 3065w, 1654s, 1615w, 1594w, 1557m, 1528m, 1498s, 1484s, 1439m, 1388w, 1345w, 1321w, 1256s, 1221s, 1200s, 1185s, 1155s, 1146s, 1122s, 1097s, 1072w, 1041w, 1027w, 1014w, 998w, 950w, 854w, 798m, 776w, 752m, 728m, 693m, 661m, 618w, 585m, 545s, 528w, 460w, 446w, 423w (Fig. S1, ESI†).

*[Tb{Ph$_2$P(O)Pyr}$_2$(hfac)$_3$] (**6**).* Yield: 0.046 g (83%). Found: C, 42.2; H, 2.2; N, 4.0%; F, 25.1%. Calcd for $C_{47}H_{29}N_4F_{18}O_8P_2Tb$ (1340.6): C, 42.1; H, 2.2; N, 4.2%; F, 25.5%. FT-IR (KBr pellets, ν/cm^{-1}): 3445w, 3065w, 1655s, 1614w, 1592w, 1558m, 1528s, 1498s, 1483s, 1439m, 1389w, 1347w, 1322w, 1256s, 1220s, 1198s, 1187s, 1156s, 1145s, 1124s, 1097s, 1072w, 1041w, 1029w, 1014m, 999w, 950w, 854w, 798m, 777w, 753m, 729m, 693m, 661m, 617w, 585m, 546s, 528w, 459w, 445w, 422w (Fig. S1, ESI†).

2.3. Characterization of the compounds

The elemental analysis (C, H, and N) was performed with a Euro EA 3000 analyzer (HEKAtech GmbH, Wegberg, Germany). Fluorine determination was performed spectrophotometrically using a Varian 50 Scan spectrophotometer. The FT-IR spectra in KBr (4000–400 cm^{-1}) were recorded using a Scimitar FTS2000 spectrophotometer. The ^{1}H (500.13 MHz) and ^{31}P{^{1}H} NMR (202.47 MHz) spectra were recorded on a Bruker Advance 500 spectrometer. The X-ray powder diffraction (XRPD) analysis was performed using a Shimadzu XRD-7000S diffractometer.

The unit cell parameters and intensities of reflections of **1** were measured at 100 K on a Bruker APEX Duo diffractometer equipped with a 4K CCD detector by standard techniques (MoKα radiation, λ = 0.71073 Å, graphite monochromator, 0.5° φ- and ω-scanning). Integration of initial experimental data and absorption correction were carried out using the APEX2 program package.[51] Diffraction data for crystals of **3** and **5** were collected at 150 K on an automated Agilent Xcalibur diffractometer equipped with an area AtlasS2 detector (MoKα radiation, λ = 0.71073 Å, graphite monochromator, 0.5° ω-scanning). The integration, absorption correction, and determination of the unit cell parameters of **3** and **5** were performed using the CrysAlisPro program package.[52] The crystallographic characteristics, experimental data, and structure refinements of **1**, **3**, and **5** are listed in Table S1 (ESI†). All non-hydrogen atoms were refined with anisotropic displacement parameters. The structures **1**, **3**, and **5** were solved using SHELXT[53] and refined by the full-matrix least-squares method on F^2 in SHELXL.[54] The N atoms of the heterocyclic moieties for all structures were localized on the basis of a higher electron density compared to the neighboring C atom positions, as well as the absence of the peaks from the H atoms. The H atoms were localized from the electron density maps and refined using a riding model. Selected interatomic distances and bond angles are given in Table S2 (ESI†). CCDC 2078495–2078497 contain the supplementary crystallographic data for **1**, **3**, and **5**, respectively.†

Photoluminescence (PL) measurements were performed on a Fluorolog 3 spectrometer (Horiba Jobin Yvon) with a cooled PC177CE-010 photon detection module equipped with an R2658 photomultiplier. The photoluminescence quantum yields (Φ_{TOT}) were measured using a Fluorolog 3 Quanta-phi device.

3. Results and discussion

3.1. Synthesis and characterization

The reactions of stoichiometric amounts of hydrated lanthanide hexafluoroacetylacetonates with the tertiary phosphine oxides in ethanol or methanol afforded mononuclear complexes with the general composition [LnL$_2$(hfac)$_3$] (L = Ph$_2$P(O)Py, Ph$_2$P(O)Pym, Ph$_2$P(O)Pyr; Ln = Eu, Tb). The use of methanol and ethanol in the syntheses results in the complexes of the same composition, however, crystals of a better quality were obtained from ethanol solution for **1** and **2** and from methanol solution for **3–6**. Note that changing the Ln^{3+} : L molar ratio from 1 : 2 to 1 : 1 and 1 : 3 did not lead to the isolation of other products apart from **1–6**.

According to the single-crystal X-ray diffraction analysis complexes **1**, **3**, and **5** crystallize in centrosymmetric space groups (Table S1, ESI†). The crystal structures of the compounds consist of isolated molecules of mononuclear complexes, whose atoms occupy the general positions (Fig. S2–S4, ESI†). The unit cell of crystal structure **1** contains two crystallographically independent molecules.

The phosphine oxides Ph$_2$P(O)Py and Ph$_2$P(O)Pyr in **1** and **5** are coordinated to the Eu atom in a monodentate mode *via* the P=O group, *i.e.*, the nitrogen atoms of azaheterocycles are not involved in the coordination (Fig. 1a and c). Thus, the coordination sphere of the Eu atom in **1** and **5** includes two O atoms of two phosphine oxide ligands with the Eu–O distances in the region of 2.32–2.34 Å for **1** and 2.32, 2.33 Å for **5**, and six O atoms of the three bidentate chelating hfac$^-$ ligands with the Eu–O distances in the region of 2.38–2.52 Å for **1** and 2.38–2.43 Å for **5** (Table S2, ESI†). The geometrical symmetry around Eu^{3+} ions was determined to be an 8-coordinated square-antiprismatic structure without an inversion center. All three chelating EuO$_2$C$_3$ rings are almost planar, and the average deviation of the atoms from their root-mean-square plane does not exceed 0.03 Å in **1** and 0.07 Å in **5**. The dihedral angles between the EuO$_2$C$_3$ rings in **1** and **5** are significantly different: one of the dihedral angles is 27.5°/22.8° in **1**, and 27.0° in **5**, and the other two dihedral angles are in the region of 81.2–97.2° in **1** and are 84.6° and

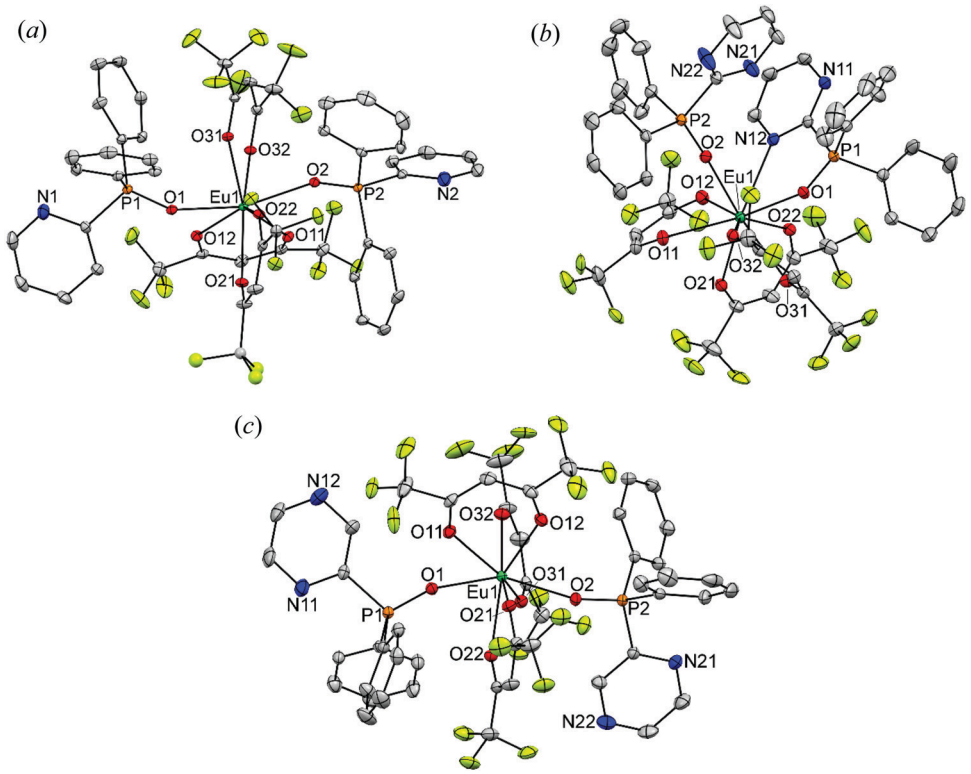

Fig. 1 Thermal ellipsoid diagram of complexes **1** (a), **3** (b), and **5** (c). Disordered atom positions and hydrogen atoms are omitted for clarity. The ellipsoids are drawn at the 30% probability level.

85.7° in **5**. The aromatic rings of phosphine oxides in both complexes are nearly planar (the average deviation from the root-mean-square atomic plane is 0.01 Å). In **1**, one of the six CF_3 groups is disordered, while all six CF_3 groups are disordered over two positions in **5**. Note that **5** is isostructural to the known complex $[Eu(Ph_3PO)_2(hfac)_3]$.[47,55] Thus, the substitution of two phenyl rings by pyrazine rings in **5** has no significant effect on the molecular structure and packing of the complex molecules in the crystal.

The experimental X-ray diffraction patterns of **1** and **5** agree well with the simulated patterns calculated from single-crystal structure data (Fig. S5, ESI†). The XRPD pattern of **2** is similar to that of **1**, indicating that they are isostructural. Compounds **5** and **6** are also isostructural (Fig. S5, ESI†).

In complex **3**, the Eu^{3+} ion is nine-coordinated by three bidentate $hfac^-$ anions (Eu–O 2.38–2.52 Å) and two ligands $Ph_2P(O)Pym$, one of which is bound to Ln in a bidentate chelating mode through the N atom of pyrimidine (Eu–N 2.82 Å) and the P═O group (Eu–O 2.37 Å), and the other acts as a monodentate O-donor ligand (Eu–O 2.38 Å). Coordination polyhedron EuN_1O_8 adopts a distorted single-cap tetragonal antiprism geometry (Fig. 1b). Two of the three chelating EuO_2C_3 rings formed upon the coordination of the $hfac^-$ ligands to the europium ion have an envelope conformation: the Eu(1) atom deviates from the O_2C_3 planes by 0.70 and 0.81 Å. The third EuO_2C_3 ring and a five-membered chelating EuOPCN ring are almost planar: the average deviations of the atoms from their root-mean-square planes do not exceed 0.02. The dihedral angles between the planes of three chelating EuO_2C_3 rings are in the region of 53.9–69.0°. The aromatic rings of the $Ph_2P(O)Pym$ ligand at P(1) are almost planar (the average deviation from the average planes does not exceed 0.01 Å). Disordering over two positions in the pyrimidine and in one of the two phenyl rings is observed at P(2). In addition, all six CF_3 groups are also disordered in two positions. Interestingly, in the previously reported nitrate complex $[Eu\{Ph_2P(O)Pym\}_2(NO_3)_3]$, both $Ph_2P(O)Pym$ act as bidentate N,O-donor ligands, while in the $[Tb\{Ph_2P(O)Pym\}_2(MeOH)(NO_3)_3]$ complex the $Ph_2P(O)Pym$ ligands are monodentate.[49] Thus, the nature of the counter-ion and the lanthanide ion has a crucial effect on the coordination mode of $Ph_2P(O)Pym$. The XRPD analysis reveals that **3** and **4** are isostructural (Fig. S5, ESI†).

In **1**, **3**, and **5**, the molecules of the complexes are assembled through F···F contacts (head-to-tail) between the disordered CF_3 groups of two neighboring molecules with distances in the region of 2.53–2.97 Å (Fig. S2–S4, ESI†). Moreover, multiple intermolecular CH···F contacts were observed for **1**, **3**, and **5** between the aromatic rings of the phosphine oxide ligands and the fluorine atoms of the $hfac^-$ ligands, and the number of these contacts per unit cell ($Z = 4$) decreases in the series $[Ln\{Ph_2P(O)Pym\}_2(hfac)_3]$ (7 contacts) > $[Ln\{Ph_2P(O)Py\}_2(hfac)_3]$ (4 contacts) = $[Ln\{Ph_2P(O)Pyr\}_2(hfac)_3]$ (4 contacts). The shortest Eu···Eu intermolecular distances are 9.84 Å for **1**, 9.80 Å for **3**, and 9.78 Å for **5**.

3.2. Photoluminescence

The emission spectra of the Eu(III) complexes **1**, **3**, and **5** in the solid state displayed in Fig. 2 contain the characteristic five

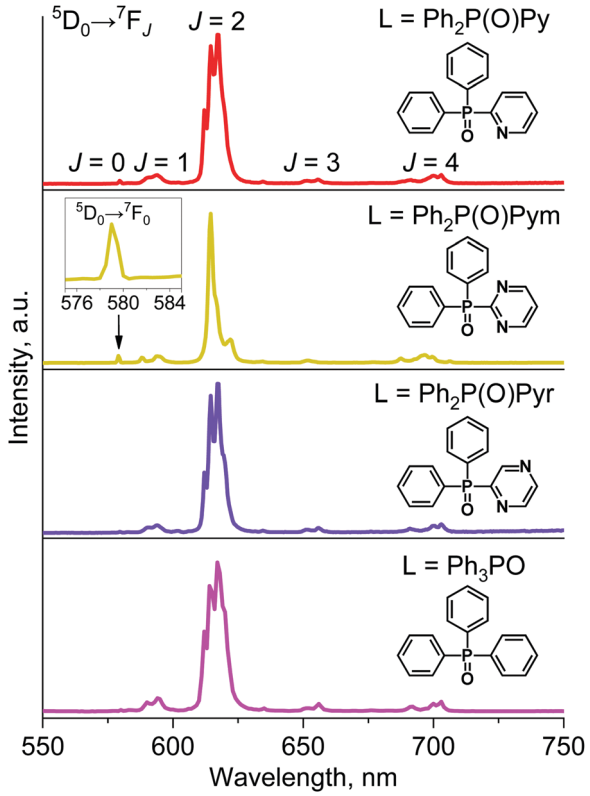

Fig. 2 Normalized photoluminescence spectra of the complexes $[EuL_2(hfac)_3]$ (L = $Ph_2P(O)Py$ (**1**), $Ph_2P(O)Pym$ (**3**), $Ph_2P(O)Pyr$ (**5**), Ph_3PO) in the solid state at 300 K (λ_{ex} = 350 nm).

narrow split emission peaks centered at 579, 594, 615, 655, and 700 nm arising from the intra-configurational $^5D_0 \rightarrow {}^7F_J$ (J = 0–4) transitions of the Eu^{3+} ion, respectively. The ligand-centered emission is not observed, indicating an efficient ligand-to-metal energy transfer process. The luminescence spectra of the Eu(III) complexes are dominated by the hypersensitive electronic dipole $^5D_0 \rightarrow {}^7F_2$ transition, the intensity of which represents 78–81% of the total integrated emission. The high relative integrated intensity of the $^5D_0 \rightarrow {}^7F_2$ transition with respect to that of the magnetic dipole $^5D_0 \rightarrow {}^7F_1$ transition (R) suggests that the Eu^{3+} ions are coordinated in a site without an inversion center (Table 1), which is consistent with the X-ray data for **1**, **3**, and **5**. The presence of only one sharp peak in the region of $^5D_0 \rightarrow {}^7F_0$ transition at 579 nm suggests the existence of a single chemical environment around the Eu^{3+} ion.[56,57]

Notably, the different coordination modes of the $Ph_2P(O)Pym$, $Ph_2P(O)Py$, and $Ph_2P(O)Pyr$ ligands in the complexes obtained are reflected in their luminescence properties, especially in the PL spectra. So, the emission spectra of $[EuL_2(hfac)_3]$ (L = $Ph_2P(O)Py$ (**1**) and $Ph_2P(O)Pyr$ (**5**)) with O-coordinated phosphine oxides are very similar in shape and show almost the same relative intensities of the different Eu^{3+} transitions. The similarity comes probably from the fact that the phosphine oxides in these complexes are coordinated to the Eu^{3+} ion to form very similar surroundings and distortion of the ion environment symmetry. At the same time, the emission spectrum of **3**, having a nine-coordinate Ln^{3+} ion, is significantly different from the emission spectra of **1** and **5**. In particular, the integrated intensity of the electronic dipole $^5D_0 \rightarrow {}^7F_2$ transition of **3** is more than 1.6 times lower than those of **1** and **5**. Interestingly, the emission spectrum of the complex $[Eu(Ph_3PO)_2(hfac)_3]$[47,55] is similar to the emission spectra of **1** and **5** (Fig. 2). Thus, the PL spectra of the Eu(III) complexes strongly depend on the coordination environment of the Eu^{3+} ion, and the substitution of a phenyl ring in Ph_3PO by pyridine and pyrazine moieties has no significant effect on the emission profile. It should be noted that the shapes and the positions of the bands in the excitation and emission spectra of the compounds $Ph_2P(O)Py$ and $Ph_2P(O)Pyr$ are similar and differ significantly from those of $Ph_2P(O)Pym$ (Fig. S6 and S7, ESI†), which could also lead to the observed differences in the photoluminescence properties of complexes **1** and **5** and complex **3**. Nevertheless, the photophysical parameters of all ligands are similar (Table S3, ESI†).

The excitation spectra of the europium(III) complexes **1**, **3**, and **5** obtained by monitoring the emission wavelength of the Eu^{3+} ions at 617 nm are similar (Fig. S8, ESI†). For all spectra, a broad band ranging from 250 to 460 nm can be seen, which is ascribed to the π–π^* electron transition of the ligands. The sharp lines at 465, 525, and 536 nm assigned to $^7F_0 \rightarrow {}^5D_{2,1}$ and $^7F_1 \rightarrow {}^5D_1$ transitions, respectively, are also seen in the solid-state excitation spectra of these complexes. However, these transitions are weaker than the absorption of the organic ligands and are overlapped by a broad excitation band, which proves that luminescence sensitization *via* excitation of the ligand is much more efficient than the direct excitation of the Eu^{3+} absorption levels.

The absolute quantum yields for the Eu^{3+} complexes in the solid state measured under ligand excitation increase in the series $Ph_2P(O)Py \approx Ph_2P(O)Pym < Ph_2P(O)Pyr$ (Table 1). In any case, compounds **1**, **3**, and **5** show significant improvement over Φ_{TOT} for $[Eu(hfac)_3(H_2O)_2]$.

The luminescence decay times for the Eu^{3+} complexes **1**, **3**, and **5** were measured at room temperature using an excitation wavelength of 350 nm and monitored by $^5D_0 \rightarrow {}^7F_2$ transition (Fig. 3). The lifetime profiles for all complexes are fitted with single exponentials, indicating that all Eu^{3+} ions occupy the same coordination environment. The luminescence lifetimes (τ_{obs}) of the $^5D_0$ level lie in the region of 718–831 μs, which is typical for europium β-diketonates (Table 1).[59–61] The photoluminescence lifetimes of the complexes are much longer than that of $[Eu(hfac)_3(H_2O)_2]$, which suggests that the Eu^{3+} ions in **1**, **3**, and **5** are well shielded from nonradiative deactivations.

Radiative lifetimes for the Eu^{3+} complexes are rather short, which explains the strong emissive properties of these compounds despite the relatively short observed lifetime (Table 1). The intrinsic quantum yields for **1**, **3**, and **5** lie in the region 68–72%, which is ~3 fold larger compared to the parent $[Eu(hfac)_3(H_2O)_2]$. The sensitization efficiencies (η_{sens}) increase 5–6 fold upon substitution of water molecules in $[Eu(hfac)_3(H_2O)_2]$ by phosphine oxides. The large radiative rate constants are due to the asymmetric coordination geometry around Eu(III) ions. The presence

Table 1 Photophysical parameters for complexes **1–6**, [Ln(hfac)$_3$(H$_2$O)$_2$] and [Ln(Ph$_3$PO)$_2$(hfac)$_3$] (Ln = Eu, Tb) in the solid state at 300 K (λ_{ex} = 350 nm)

Compound	τ_{obs} [a] (μs)	τ_{rad} [b] (μs)	Φ_{Ln} [c] (%)	Φ_{TOT} [d] (%)	η_{sens} [e]	R [f]	k_r [g] (s^{-1})	k_{nr} [h] (s^{-1})
[Eu{Ph$_2$P(O)Py}$_2$(hfac)$_3$] (**1**)	763	1065	72	43	0.60	15.4	939	372
[Tb{Ph$_2$P(O)Py}$_2$(hfac)$_3$] (**2**)	418	n.a.	n.a.	31	n.a.	n.a.	n.a.	n.a.
[Eu{Ph$_2$P(O)Pym}$_2$(hfac)$_3$] (**3**)	831	1205	68	44	0.65	13.2	930	373
[Tb{Ph$_2$P(O)Pym}$_2$(hfac)$_3$] (**4**)	358	n.a.	n.a.	29	n.a.	n.a.	n.a.	n.a.
[Eu{Ph$_2$P(O)Pyr}$_2$(hfac)$_3$] (**5**)	718	993	72	56	0.78	16.3	1007	386
[Tb{Ph$_2$P(O)Pyr}$_2$(hfac)$_3$] (**6**)	443	n.a.	n.a.	39	n.a.	n.a.	n.a.	n.a.
[Eu(Ph$_3$PO)$_2$(hfac)$_3$]	741	928	80	54	0.68	16.8	1078	272
[Tb(Ph$_3$PO)$_2$(hfac)$_3$]	96	n.a.	n.a.	10	n.a.	n.a.	n.a.	n.a.
[Eu(hfac)$_3$(H$_2$O)$_2$]	326	1389	24	3	0.13	11.3	720	2348
[Tb(hfac)$_3$(H$_2$O)$_2$]	536	n.a.	n.a.	50	n.a.	n.a.	n.a.	n.a.

[a] Lifetimes measured in the solid state. [b] Radiative lifetimes for Eu^{3+} complexes calculated as $\tau_{rad} = 1/n^3A_{MD,0} \times I_{MD}/I_{TOT}$, where $A_{MD,0}$ is the spontaneous emission probability for $^5D_0 \rightarrow {}^7F_1$ transition *in vacuo* (14.65 s^{-1}), and n is the refractive index of the medium (an average index of refraction equal to 1.5 was used).[58] [c] Intrinsic quantum yields calculated as $\Phi_{Ln} = \tau_{obs}/\tau_{rad}$. [d] Total absolute quantum yields measured in the solid state. [e] Energy transfer efficiencies between the ligand and the Eu^{3+} ion calculated as $\eta_{sens} = \Phi_{TOT}/\Phi_{Ln}$. [f] Ratios R calculated from the formula $I(^5D_0 \rightarrow {}^7F_2)/I(^5D_0 \rightarrow {}^7F_1)$. [g] The radiative rate constants calculated as $1/\tau_{rad}$. [h] The non-radiative rate constants calculated as $1/\tau_{obs} - 1/\tau_{rad}$.

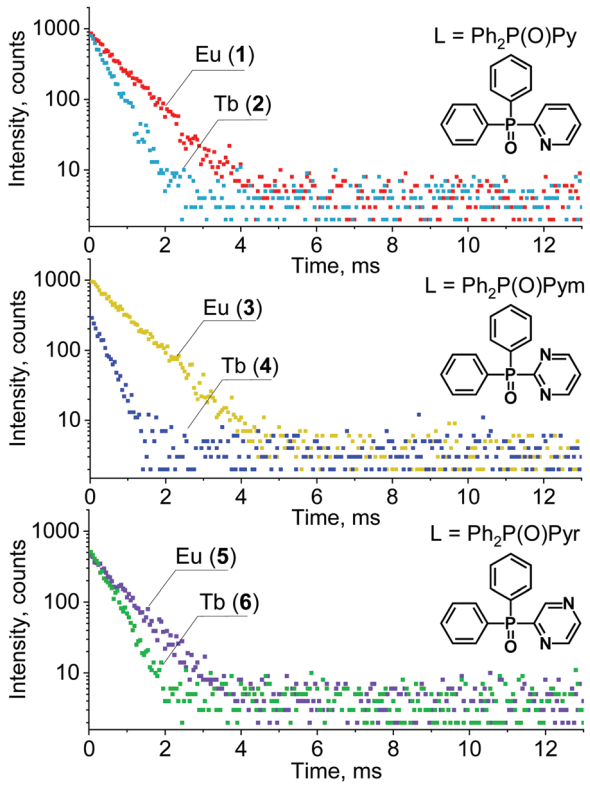

Fig. 3 Kinetics of photoluminescence decay of the complexes [LnL$_2$(hfac)$_3$] (Ln = Eu, Tb; L = Ph$_2$P(O)Py, Ph$_2$P(O)Pym, Ph$_2$P(O)Pyr) in the solid state at 300 K.

of multiple intra- and intermolecular CH...F contacts in the europium complexes leads to low nonradiative rate constants (k_{nr}) by forming low-vibrational coordination structures. It should be noted that the photophysical parameters of [Eu(Ph$_3$PO)$_2$(hfac)$_3$] are close to those of **5**, which is apparently due to the fact that these complexes are isostructural.

The emission spectra of the Tb(III) complexes **2**, **4**, and **6** show characteristic peaks at 485–496, 544, 580–590, 615–624, and 647–657 nm, which are assigned to the transitions from $^5D_4$ to ^7F_J (J = 6–2), with the emission at 544 nm being the strongest (Fig. 4). The Stark splitting shapes at 544 nm ($^5D_4 \rightarrow {}^7F_5$) for **2**, **6** and the known complex [Tb(Ph$_3$PO)$_2$(hfac)$_3$][47] are similar, which indicates the same coordination geometry in these complexes. A broad ligand-centered band in the excitation spectra of the Tb(III) complexes **2**, **4**, and **6** confirms energy transfer from ligands to metal (Fig. S9, ESI†). The direct excitation peak of low intensity corresponding to the $^7F_6 \rightarrow {}^5D_4$ transition could also be observed at 485 nm.

The quantum yields of the terbium complexes are lower than the quantum yields of the europium complexes (Table 1). The emission decays of **2**, **4**, and **6** showed microsecond-scale emission lifetimes by estimating single-exponential fittings. In contrast to the analogous isostructural Eu(III) complexes with similar photophysical parameters, the quantum yield and the luminescence lifetime of **6** are much greater than those of [Tb(Ph$_3$PO)$_2$(hfac)$_3$], which is due to the fact that these Tb(III) complexes have different crystal structures.

3.3. Triboluminescence

We observed the triboluminescence (TL) of all prepared Eu(III) and Tb(III) complexes in the dark at 300 K in air. The complexes **1–6** exhibit TL despite their nonchiral space groups, suggesting that intermolecular structure is the dominant factor for TL activity. The F···F contacts (Fig. S2–S4, ESI†) are also related to the TL activity of the complexes since they could prevent the formation of strong hydrogen bonds between the molecules. Among complexes **1–6**, the TL activity was qualitatively higher in **1**, **5**, and **6** (ESI,† Video). For all complexes, the hydrogen atoms of aromatic cycles and fluorine atoms of the hfac$^-$ ligands form CH···F contacts (Fig. S2–S4, ESI†). Since the number of intermolecular CH···F contacts for [Ln{Ph$_2$P(O)Pym}$_2$(hfac)$_3$] (7 contacts) is greater than for [LnL$_2$(hfac)$_3$], where L = Ph$_2$P(O)Py and Ph$_2$P(O)Pyr, (4 contacts), the mechanical stability of these compounds was assumed to be [Ln{Ph$_2$P(O)Pym}$_2$(hfac)$_3$] > [Ln{Ph$_2$P(O)Py}$_2$(hfac)$_3$] ≈ [Ln{Ph$_2$P(O)Pyr}$_2$(hfac)$_3$]. Thus, the observed TL activity is inversely proportional to the mechanical stability. The similar dependence of triboluminescent activity on mechanical stability is demonstrated in ref. 18. The weak TL of **2** can be attributed to its relatively low quantum yield (Table 1).

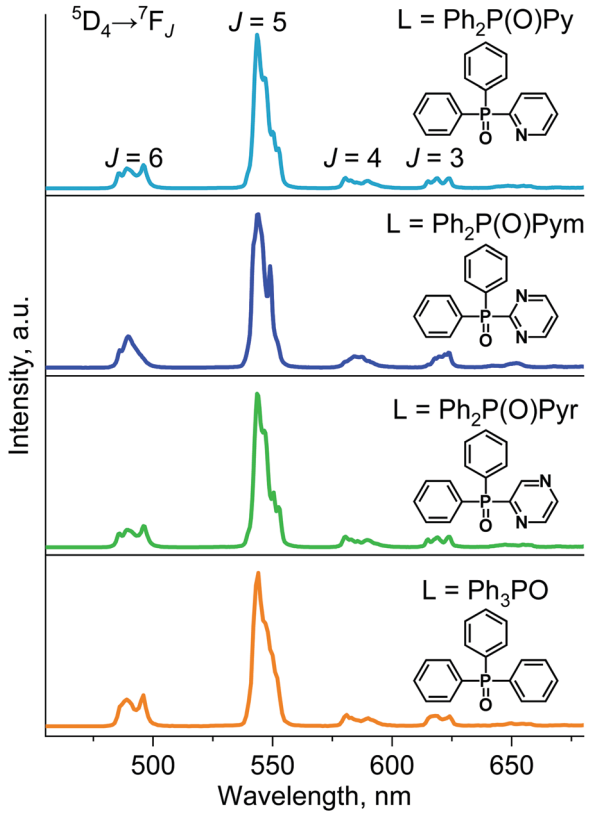

Fig. 4 Normalized photoluminescence spectra of the complexes $[TbL_2(hfac)_3]$ (L = $Ph_2P(O)Py$ (**2**), $Ph_2P(O)Pym$ (**4**), $Ph_2P(O)Pyr$ (**6**), Ph_3PO) in the solid state at 300 K (λ_{ex} = 350 nm).

It should be noted that triboluminescence for $[Eu(Ph_3PO)_2(hfac)_3]$ was previously described.[62] Since the complexes $[Eu(Ph_3PO)_2(hfac)_3]$ and $[Eu\{Ph_2P(O)Pyr\}_2(hfac)_3]$ are isostructural, they seem to have a similar triboluminescent activity. Thus, the above observations indicate that the ability to generate TL depends on the proportion of the intermolecular contacts in the crystal structures and the mechanical stability of the compounds.

4. Conclusions

In summary, we have designed, synthesized, and characterized a family of centrosymmetric Eu(III) and Tb(III) complexes composed of low-vibrational frequency hexafluoroacetylacetonate ions and phosphine oxide ligands containing various azaheterocycles. X-ray diffraction analysis showed that the coordination mode of phosphine oxide depends on the nature of the N-heterocycle included in its composition. Due to the high energy transfer efficiency, high overall quantum yields up to 56% were obtained for the Eu(III) complexes in the solid state. The complexes exhibit triboluminescence under ambient conditions despite their nonchiral space groups. The intensity of triboluminescence is inversely proportional to the number of C–H···F contacts in the crystal structures indicating that intermolecular structure is one of the main factors influencing TL activity.

Conflicts of interest

The authors declare that they have no known competing financial interests or personal relationships that could have appeared to influence the work reported in this paper.

Acknowledgements

The authors thank the Multi-Access Chemical Research Centre SB RAS for spectral and analytical measurements and XRD Facility of NIIC SB RAS for the data collection. The work was supported by the Russian Foundation for Basic Research (project no. 19-73-00158).

References

1 A. W. G. Platt, *Coord. Chem. Rev.*, 2017, **340**, 62–78.
2 Y. Hirai, T. Nakanishi and Y. Hasegawa, *J. Lumin.*, 2016, **170**, 801–807.
3 J. C. G. Bünzli, *Coord. Chem. Rev.*, 2015, **293–294**, 19–47.
4 Y. Hasegawa, Y. Kitagawa and T. Nakanishi, *NPG Asia Mater.*, 2019, **10**, 52–70.
5 H. Iwanaga and F. Aiga, *ACS Omega*, 2021, **6**, 416–424.
6 T. Harada, Y. Hasegawa, Y. Nakano, M. Fujiki, M. Naito, T. Wada, Y. Inoue and T. Kawai, *J. Alloys Compd.*, 2009, **488**, 599–602.
7 M. Congiu, M. Alamiry, O. Moudam, S. Ciorba, P. R. Richardson, L. Maron, A. C. Jones, B. S. Richards and N. Robertson, *Dalton Trans.*, 2013, **42**, 13537–13545.
8 S. Miyazaki, K. Miyata, H. Sakamoto, F. Suzue, Y. Kitagawa, Y. Hasegawa and K. Onda, *J. Phys. Chem. A*, 2020, **124**, 6601–6606.
9 H. Iwanaga, *J. Lumin.*, 2018, **200**, 233–239.
10 H. Xu, L.-H. Wang, X.-H. Zhu, K. Yin, G.-Y. Zong, X.-Y. Hou and W. Huang, *J. Phys. Chem. B*, 2006, **110**, 3023–3029.
11 H. Xu, K. Yin and W. Huang, *Chem. – Eur. J.*, 2007, **13**, 10281–10293.
12 Md. A. Subhan, Y. Hasegawa, T. Suzuki, S. Kaizaki and Y. Shozo, *Inorg. Chim. Acta*, 2009, **362**, 136–142.
13 V. Divya, R. O. Freire and M. L. P. Reddy, *Dalton Trans.*, 2011, **40**, 3257–3268.
14 D. B. A. Raj, B. Francis, M. L. P. Reddy, R. R. Butorac, V. M. Lynch and A. H. Cowley, *Inorg. Chem.*, 2010, **49**, 9055–9063.
15 S. Mal, M. Pietraszkiewicz and O. Pietraszkiewicz, *J. Coord. Chem.*, 2015, **68**, 367–377.
16 S. Biju, N. Gopakumar, J.-C. G. Bünzli, R. Scopelliti, H. K. Kim and M. L. P. Reddy, *Inorg. Chem.*, 2013, **52**, 8750–8758.
17 Y. Kitagawa, A. Naito, K. Fushimi and Y. Hasegawa, *Chem. – Eur. J.*, 2021, **27**, 2279–2283.
18 Y. Hirai, P. P. Ferreira da Rosa, T. Nakanishi, Y. Kitagawa, K. Fushimi, T. Seki, H. Ito and Y. Hasegawa, *Inorg. Chem.*, 2018, **57**, 14653–14659.
19 Y. Hirai, T. Nakanishi, Y. Kitagawa, K. Fushimi, T. Seki, H. Ito and Y. Hasegawa, *Angew. Chem.*, 2017, **129**, 7277–7281.
20 S. V. Eliseeva, D. N. Pleshkov, K. A. Lyssenko, L. S. Lepnev, J.-C. G. Bünzli and N. P. Kuzmina, *Inorg. Chem.*, 2010, **49**, 9300–9311.

21 H.-Y. Wong, W.-S. Lo, W. T. K. Chan and G.-L. Law, *Inorg. Chem.*, 2017, **56**, 5135–5140.
22 B. V. Bukvetskii and I. V. Kalinovskaya, *J. Fluoresc.*, 2017, **27**, 773–779.
23 B. V. Bukvetskii, N. V. Petrochenkova and A. G. Mirochnik, *Russ. Chem. Bull.*, 2015, **64**, 2427–2432.
24 Y. Hirai, T. Nakanishi, K. Miyata, K. Fushimi and Y. Hasegawa, *Mater. Lett.*, 2014, **130**, 91–93.
25 K. Miyata, Y. Konno, T. Nakanishi, A. Kobayashi, M. Kato, K. Fushimi and Y. Hasegawa, *Angew. Chem., Int. Ed.*, 2013, **52**, 6413–6416.
26 Y. Kitagawa, M. Kumagai, P. P. Ferreira da Rosa, K. Fushimi and Y. Hasegawa, *Chem. – Eur. J.*, 2021, **27**, 264–269.
27 Y. Hasegawa and Y. Kitagawa, *J. Mater. Chem. C*, 2019, **7**, 7494–7511.
28 M. Yamamoto, Y. Kitagawa, T. Nakanishi, K. Fushimi and Y. Hasegawa, *Chem. – Eur. J.*, 2018, **24**, 17719–17726.
29 K. Miyata, T. Nakanishi, K. Fushimi and Y. Hasegawa, *J. Photochem. Photobiol., A*, 2012, **235**, 35–39.
30 Y. Kitagawa, R. Ohno, T. Nakanishi, K. Fushimia and Y. Hasegawa, *Photochem. Photobiol. Sci.*, 2017, **16**, 683–689.
31 L. J. Charbonniere, R. Ziessel, M. Montalti, L. Prodi, N. Zaccheroni, C. Boehme and G. Wipff, *J. Am. Chem. Soc.*, 2002, **124**, 7779–7788.
32 C. Wei, B. Sun, Z. Zhao, Z. Cai, J. Liu, Y. Tan, H. Wei, Z. Liu, Z. Bian and C. Huang, *Inorg. Chem.*, 2020, **59**, 8800–8808.
33 Y. Hasegawa, R. Hieda, K. Miyata, T. Nakagawa and T. Kawai, *Eur. J. Inorg. Chem.*, 2011, 4978–4984.
34 L. Prodi, M. Montalti, N. Zaccheroni, G. Pickaert, L. Charbonniere and R. Ziessel, *New J. Chem.*, 2003, **27**, 134–139.
35 M. Pietraszkiewicz, A. Kłonkowski, K. Staniszewski, J. Karpiuk and S. Bianketti, *J. Alloys Compd.*, 2004, **380**, 241–247.
36 O. Pietraszkiewicz, M. Pietraszkiewicz, J. Karpiuk and M. Jesie, *J. Rare Earths*, 2009, **27**, 584–587.
37 N. E. Borisova, A. V. Kharcheva, S. V. Patsaeva, L. A. Korotkov, S. Bakaev, M. D. Reshetova, K. A. Lyssenko, E. V. Belova and B. F. Myasoedov, *Dalton Trans.*, 2017, **46**, 2238–2248.
38 Z. Spichal, M. Necas, J. Pinkas and J. Novosad, *Inorg. Chem.*, 2004, **43**, 2776–2778.
39 B. G. Vats, S. Kannan, M. Kumar and M. G. B. Drew, *ChemistrySelect*, 2017, **2**, 3683–3689.
40 I. Sage and G. Bourhill, *J. Mater. Chem.*, 2001, **11**, 231–245.
41 D.-P. Li, C.-H. Li, J. Wang, L.-C. Kang, T. Wu, Y.-Z. Li and X.-Z. You, *Eur. J. Inorg. Chem.*, 2009, 4844–4849.
42 G. E. Hardy, W. C. Kaska, B. P. Chandra and J. I. Zink, *J. Am. Chem. Soc.*, 1981, **103**, 1074–1079.
43 X.-F. Chen, C.-Y. Duan, X.-H. Zhu, X.-Z. You, S. S. S. Raj, H.-K. Fun and J. Wuc, *Mater. Chem. Phys.*, 2001, **72**, 11–15.
44 X.-L. Li, Y. Zheng, J.-L. Zuo, Y. Song and X.-Z. You, *Polyhedron*, 2007, **26**, 5257–5262.
45 X.-F. Chen, X.-H. Zhu, Y.-H. Xu, S. S. S. Raj, S. Öztürk, H.-K. Fun, J. Ma and X.-Z. You, *J. Mater. Chem.*, 1999, **9**, 2919–2922.
46 M. F. Richardson, W. F. Wagner and D. E. Sands, *J. Inorg. Nucl. Chem.*, 1968, **30**, 1275–1289.
47 V. A. Petrov, W. J. Marshall and V. V. Grushin, *Chem. Commun.*, 2002, 520–521.
48 M. I. Rogovoy, M. P. Davydova, I. Y. Bagryanskaya and A. V. Artem'ev, *Mendeleev Commun.*, 2020, **30**, 305–307.
49 Yu. A. Bryleva, A. V. Artem'ev, L. A. Glinskaya, D. G. Samsonenko, M. I. Rakhmanova, M. P. Davydova and K. M. Yzhikova, *J. Struct. Chem.*, 2021, **62**, 265–276.
50 R. M. Denton, J. An, B. Adeniran, A. J. Blake, W. Lewis and A. M. Poulton, *J. Org. Chem.*, 2011, **76**, 6749–6767.
51 Bruker AXS Inc. (2000–2012). APEX2 (Version 2.0), Bruker Advanced X-ray Solutions. Madison, Wisconsin, USA.
52 CrysAlisPro Software system, version 1.171.39.46. Rigaku Oxford Diffraction, Rigaku Corporation, Wrocław, Poland, 2018.
53 G. M. Sheldrick, *Acta Crystallogr., Sect. A: Found. Adv.*, 2015, **71**, 3–8.
54 G. M. Sheldrick, *Acta Crystallogr., Sect. C: Struct. Chem.*, 2015, **71**, 3–8.
55 E. S. Panin, V. E. Karasev and I. V. Kalinovskaya, *Koord. Khim.*, 1988, **14**, 513–518.
56 J. Kai, F. D. Parra and H. F. Brito, *J. Mater. Chem.*, 2008, **18**, 4549–4554.
57 S. Biju, M. L. P. Reddy, A. H. Cowley and K. V. Vasudevan, *Cryst. Growth Des.*, 2009, **9**, 3562–3569.
58 M. H. V. Werts, R. T. F. Jukes and J. W. Verhoeven, *Phys. Chem. Chem. Phys.*, 2002, **4**, 1542–1548.
59 S. A. Bhata and K. Iftikhar, *New J. Chem.*, 2019, **43**, 13162–13172.
60 V. I. Tsaryuk, K. P. Zhuravlev, R. Szostak and A. V. Vologzhanina, *J. Struct. Chem.*, 2020, **61**, 1026–1037.
61 G. B. V. Lima, J. C. Bueno, A. F. da Silva, A. N. C. Neto, R. T. Moura Jr, E. E. S. Teotonio, O. L. Malta and W. M. Faustino, *J. Lumin.*, 2020, **219**, 116884.
62 I. V. Kalinovskaya and A. G. Mirochnik, *Russ. J. Phys. Chem. A*, 2014, **88**, 541–543.

